

1 **Mapping global onshore wind turbines using multi-source remote**  
2 **sensing images and hybrid learning approaches**

3 Shujun Li<sup>1,6</sup>, Jianchuan Qi<sup>2,3,4,\*</sup>, Yongze Song<sup>5</sup>, Peng Wang<sup>1,6,\*</sup>

4

5 1. State Key Laboratory for Ecological Security of Regions and Cities, Institute of  
6 Urban Environment, Chinese Academy of Sciences, Xiamen, Fujian 361021, China

7 2. School of Environment, Tsinghua University, Beijing, 100084, China

8 3. Institute for Carbon Neutrality, Tsinghua University, Beijing, 100084, China

9 4. TianGong Think Tank, Research Institute for Environmental Innovation (Suzhou)  
10 Tsinghua, 215163, China

11 5. School of Design and the Built Environment, Curtin University, Perth, Australia

12 6. University of Chinese Academy of Sciences, Beijing, 100049, China

13

14 \* To whom correspondence may be addressed.

15 *Correspondence to:* [pwang@iue.ac.cn](mailto:pwang@iue.ac.cn), [jcqi@tsinghua.edu.cn](mailto:jcqi@tsinghua.edu.cn)

16

17

18

19

20

21

22

23

24

25

26

27

28

29

30

31

32

33 **Abstract.** Wind power serves as a vital zero-carbon alternative to fossil fuels for  
34 climate change mitigation. Nevertheless, the vast expansion of wind turbine installation  
35 requires extensive terrestrial resources, raising wide concerns regarding land use  
36 competition and ecological impacts. Quantifying these effects necessitates near real-  
37 time geospatial data on wind turbine placement and density. However, current methods  
38 remain inadequate for monitoring the fast-growing wind turbine deployment. Here, we  
39 developed an integrated framework that combines OpenStreetMap (OSM) data with  
40 multi-source remote sensing images (Google Earth and Sentinel-1/2) and deep learning  
41 and traditional machine learning models (ResNet-18 and Random Forest) to map global  
42 onshore wind turbines. Our models achieve validation accuracy >97% while enabling  
43 cost-effective, timely updates of global onshore wind turbines. Eventually, we  
44 established a geographical dataset (GonshoreWT2024) covering a total of 416,532  
45 wind turbines globally by 2024. This dataset represents a tenfold expansion over global  
46 wind turbine inventories as of 2020, and updates 42,955 more onshore wind turbines  
47 compared to the Global Renewables Watch based on lower computational requirements.  
48 In addition, we found that 87% wind turbines are situated on cropland and grassland,  
49 followed by forest and bare ground. This dataset facilitates essential studies on  
50 renewable energy land management, ecological impact analysis, and data-driven energy  
51 transition policies. The codes and dataset of the global onshore wind turbines are  
52 available at the Zenodo link: <https://doi.org/10.5281/zenodo.18984175> (Shujun et al.,  
53 2025).

54

## 55 **1 Introduction**

56 Wind energy will increase substantially over the coming decades to meet clean energy  
57 targets (Mckenna et al., 2025). Under the 1.5°C scenario, global installed wind power  
58 capacity is projected to reach nearly 10,300 GW by 2050, with onshore wind  
59 comprising 75% of total installations (Raimi et al., 2023). Compared to other energy  
60 technologies, wind power exhibits relatively low land use efficiency when accounting  
61 for wind turbine spacing requirements (Dai et al., 2024). Accordingly, meeting future  
62 deployment targets will necessitate substantial land allocations, raising pressing  
63 concerns about land-use conversion and biodiversity loss that demand urgent attention  
64 (Kati et al., 2021; Rinne et al., 2018). However, detailed geospatial data at the facility  
65 level is particularly required for the quantification of these impacts (Kruitwagen et al.,  
66 2021).

67 Indeed, asset-level data and facility arrangement are essential for power generation  
68 nowcasting and forecasting, as well as for decision-making by grid operators and  
69 energy stakeholders (Calvert et al., 2013; Tavakkoli et al., 2021). For instance,  
70 geospatial analysis of historical placements can inform wind turbine siting decisions by  
71 revealing both human and environmental landscape factors (Roddis et al., 2018).  
72 Previous research confirmed that substantial positional errors exist in the current  
73 available wind facility records, especially pronounced in high-growth renewable energy  
74 markets (Cerri et al., 2024; Effenberger and Ludwig, 2022). A timely geospatial data

75 set is critically needed to maintain accurate records of wind energy infrastructure, given  
76 its unprecedented growth rate. The dataset could also support data-driven metrics for  
77 Sustainable Development Goals (SDGs) (Mishra et al., 2024), including SDG 7  
78 (Affordable and Clean Energy), SDG 13 (Climate Action), and SDG 15 (Life on Land).

79 Despite the demonstrated importance of location data, only a few spatially explicit  
80 datasets are publicly available. At the global scale, a geospatial wind turbine dataset for  
81 2020 is introduced (Dunnnett et al., 2020), but its update mechanism depends entirely on  
82 OpenStreetMap (OSM), a crowdsourced data derived from heterogeneous contributors  
83 that could introduce significant uncertainty. Meanwhile, while multiple frameworks  
84 exist for updating global offshore wind turbine data (Hoeser et al., 2022; Zhang et al.,  
85 2021), onshore wind turbine updating methods remain underdeveloped due to their  
86 greater spatial distribution and environmental variability. Recently, Microsoft and  
87 Planet's Global Renewables Watch platform employs deep learning for global wind and  
88 solar monitoring (Robinson et al., 2025), but it demands massive computing resources  
89 for data updates. At the national level, there are geospatial datasets for the United States  
90 (Rand et al., 2020), Germany (Manske et al., 2022), Italy (Smeraldo et al., 2020), and  
91 South Africa (Kleebauer et al., 2025). However, inconsistent data collection methods  
92 across datasets with delays in update frequencies could hinder their systematic  
93 comparability. Currently, the research community lacks both a unified methodology and  
94 accessible datasets for tracking worldwide onshore wind turbine deployments.

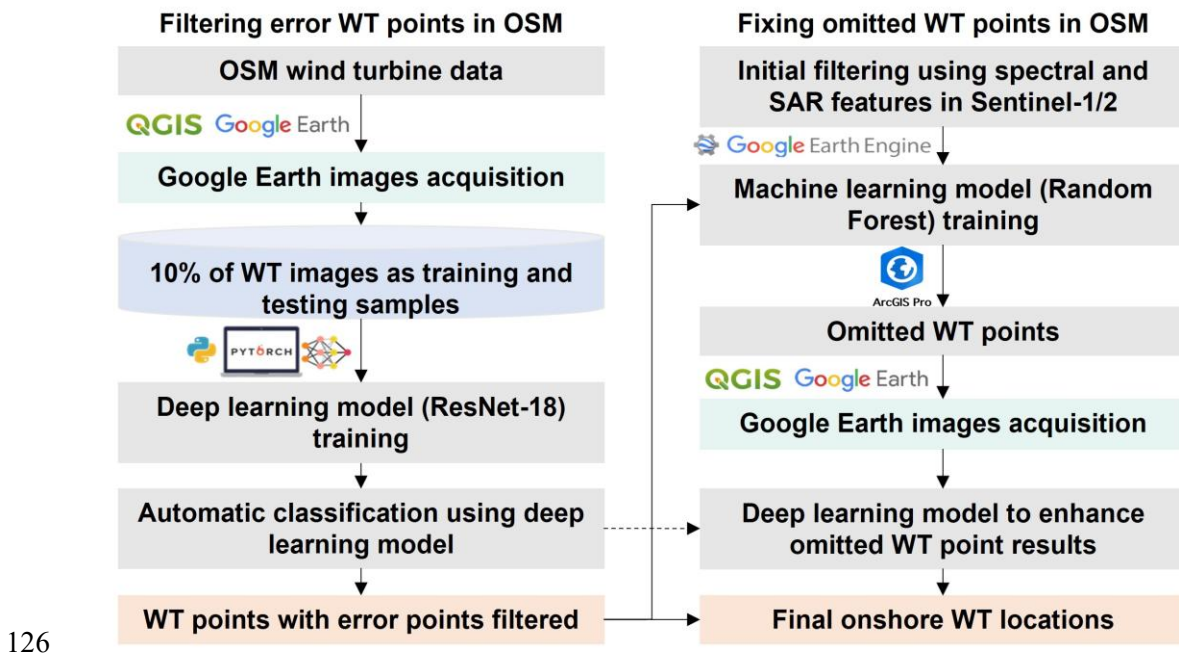
95 To address these gaps, our study presents a hybrid framework combining deep learning  
96 and a traditional machine learning framework for updating global onshore wind turbine  
97 data. By integrating multi-source remote sensing data (Google Earth high-resolution  
98 images, Sentinel-1, and Sentinel-2), our workflow systematically detects and validates  
99 global onshore wind turbines to generate a 2024 geodatabase (GonshoreWT2024). With  
100 OSM wind turbine locations as initial inputs, the two-stage locating process involves:  
101 (1) training a deep learning classifier (ResNet-18) on Google high-resolution images to  
102 identify and correct erroneous OSM records, followed by (2) detecting omitted wind  
103 turbines with Sentinel-1/2 spectral features and a Random Forest model trained on  
104 Google Earth Engine (GEE). Additionally, we examined worldwide land use  
105 characteristics of wind turbine sites and their national distribution patterns to assess  
106 current wind energy spatial utilization. Our study delivers comprehensive monitoring  
107 tools and datasets essential for tracking wind energy growth, enabling data-driven  
108 policy decisions to advance sustainable wind power development worldwide.

109

110 **2 Materials and methods**

111 **2.1 Framework**

112 The proposed framework combines OSM's crowdsourced geospatial data with a two-  
113 stage deep learning/traditional machine learning pipeline (**Figure 1**) to locate a global  
114 onshore wind turbine dataset for 2024. The first part involves utilizing OSM wind  
115 turbine coordinates to extract high-resolution Google Earth images, then training a  
116 ResNet-18 convolutional neural network to classify and flag erroneous wind turbines  
117 in the OSM dataset. The second part employs confirmed wind turbine locations to train  
118 a Random Forest classifier for potential omitted wind turbines using Sentinel-1/2  
119 features at GEE, combining with validation through our pre-trained ResNet-18 model  
120 applied to Google high-resolution images of the potential points. The integrated output  
121 merges error-corrected OSM data with supplemented wind turbine omissions,  
122 generating an enhanced global dataset that demonstrates improved spatial accuracy and  
123 comprehensive operational wind turbine coverage. This framework reduces barriers to  
124 entry by using publicly available platforms, offering a cost-saving and resource-  
125 efficient alternative.



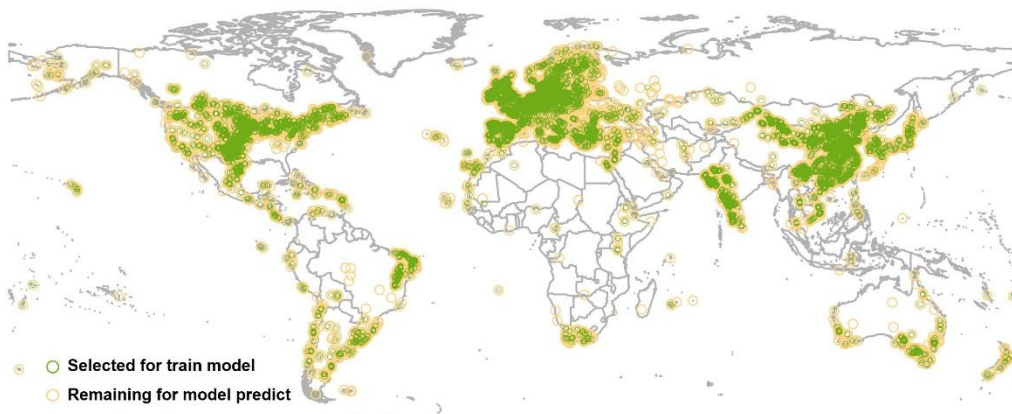
126  
127 **Figure 1.** Framework for mapping global onshore wind turbines. Where the WT  
128 represents wind turbines, OSM represents OpenStreetMap (© OpenStreetMap  
129 contributors, <https://www.openstreetmap.org/copyright>).

130 **2.2 Two-phase approach for global onshore wind turbine mapping**

131 **2.2.1 Filtering of erroneous data with deep learning model**

132 We obtained the baseline OSM 2024 wind turbine dataset through the QuickOSM  
133 plugin (based on the Overpass API) in QGIS software with the query parameter:

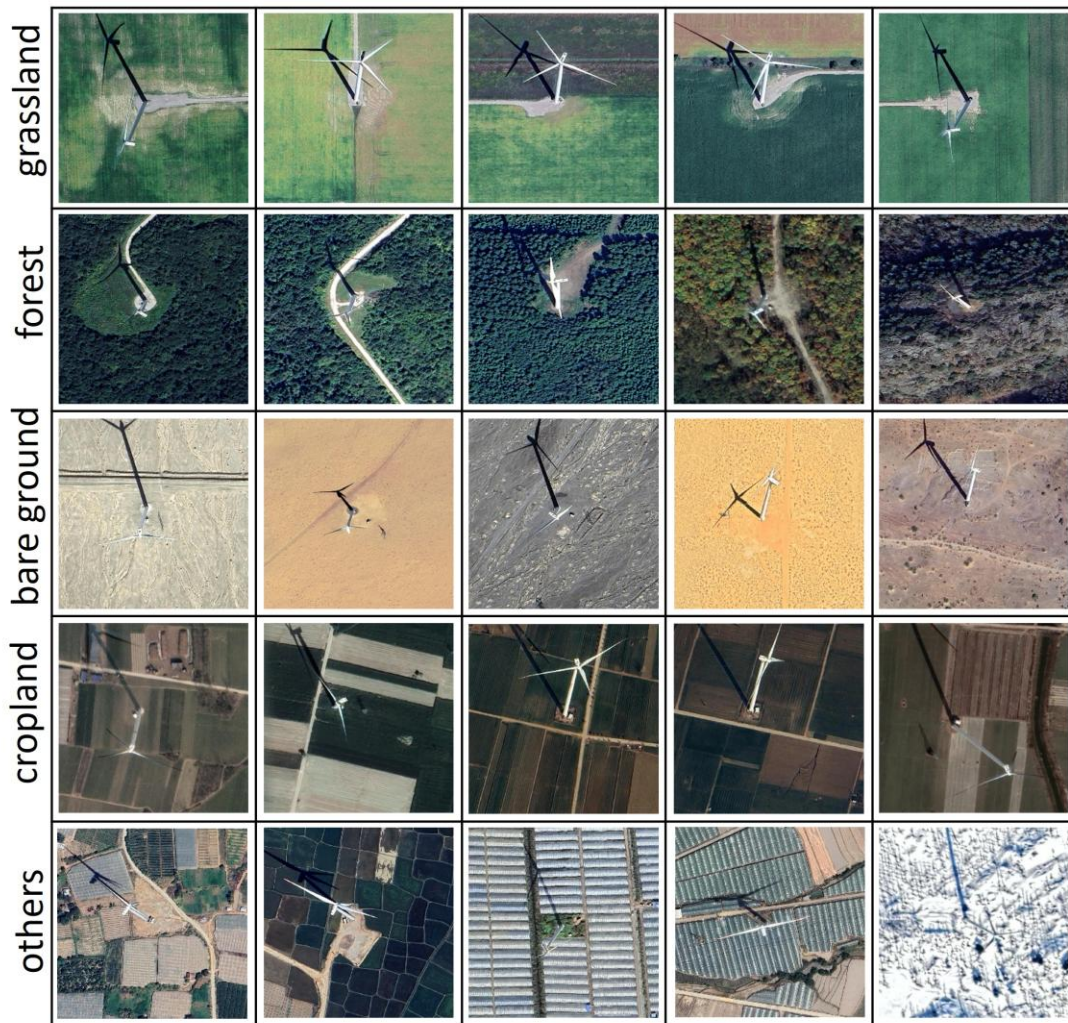
134 generator: source=wind. Given our focus on the individual wind turbine level, we  
135 utilized this query filter for nodes representing wind turbines in the format of point  
136 features. Since we focus on onshore wind turbines, the OSM land polygon derived from  
137 <https://osmdata.openstreetmap.de/data/land-polygons.html> is used to define the study  
138 extent and refine the dataset. A preliminary global inventory of 377,154 geolocated  
139 onshore wind turbines with complete metadata records. Given OSM's crowdsourced  
140 feature due to unverified contributors, the extracted wind turbine locations serve as  
141 initial references that demand thorough validation. Subsequent analysis regarding  
142 addressing both commission errors (false positives) and omission errors (omitted wind  
143 turbines) through technical verification.



145 **Figure 2.** Spatial distribution of training samples (green points).

146 Based on the OSM-derived wind turbine coordinates, we generated 500m×500m  
147 extraction zones to acquire high-resolution Google Earth images through the Buffer  
148 Tool in QGIS software. This conservative spatial buffer accounts for maximum wind  
149 turbine diameters ( $\leq 200\text{m}$ ) while guaranteeing full rotor coverage (Muller et al., 2024).  
150 The image tiles were resized to a standardized 256×256-pixel format, maintaining  
151 optimal input dimensions for our ResNet-18 architecture while retaining essential wind  
152 turbine characteristics. For model construction, we employed a strategically sampled  
153 10% subset (37,285 images) from the complete dataset, which balances  
154 representativeness with computational constraints during training. The spatial  
155 distribution of sampled wind turbine points exhibits balanced representation across  
156 global regions in **Figure 2**, confirming our stratified random sampling approach  
157 effectively maintained geographic diversity. This subset was manually annotated with  
158 labels for 'wind turbines' and 'non-turbines'. The labeled data was then split into a  
159 training set (60%, 22,372 images), a testing set (20%, 7,457 images), and a validation  
160 set (20%, 7,456 images) for our OSM error classification model. Representative  
161 samples of the buffered wind turbine images are displayed in **Figure 3**. The visual data  
162 reveal that wind turbines are distributed across diverse landscapes, including grasslands,  
163 bare land, cropland, and forests, with occasional installations near water bodies and  
164 built environments.

165



© 2024 Google Earth

166

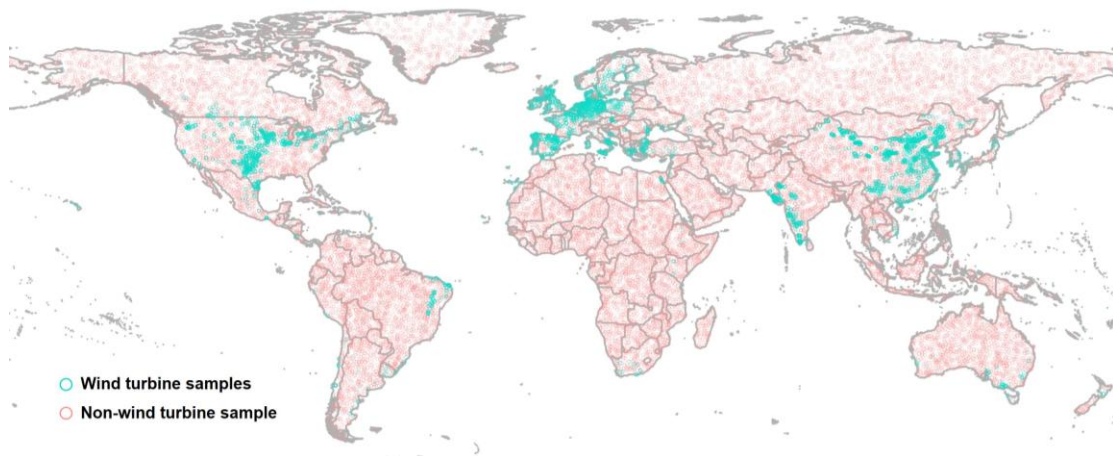
167 **Figure 3.** Different land types of onshore wind turbines in Google Earth images  
 168 (Imagery © 2024 Vanter, Map data © 2024 Google, Maxar Technologies).

169 For automated classification of OSM wind turbine data, we employed the ResNet-18  
 170 architecture (He et al., 2016), leveraging its demonstrated image classification  
 171 capabilities while ensuring computational efficiency for geospatial applications at scale.  
 172 Our optimized ResNet-18 model processed all 339,869 candidate images, identifying  
 173 291,501 confirmed wind turbine locations (85.8% positive rate) while classifying  
 174 48,368 as non-turbine cases (14.2%). All negative classifications underwent rigorous  
 175 cross-platform verification using Google Earth, Bing Maps, and Sentinel-2 images,  
 176 enabling the removal of inaccurate OSM entries. These validated results were then  
 177 integrated with the training data to generate an enhanced global wind turbine dataset  
 178 with improved accuracy. The dataset and codes for training the model are available at  
 179 the Zenodo website: <https://doi.org/10.5281/zenodo.18984175> (Shujun et al., 2025).

### 180 2.2.2 Supplementing omitted data with traditional machine learning model

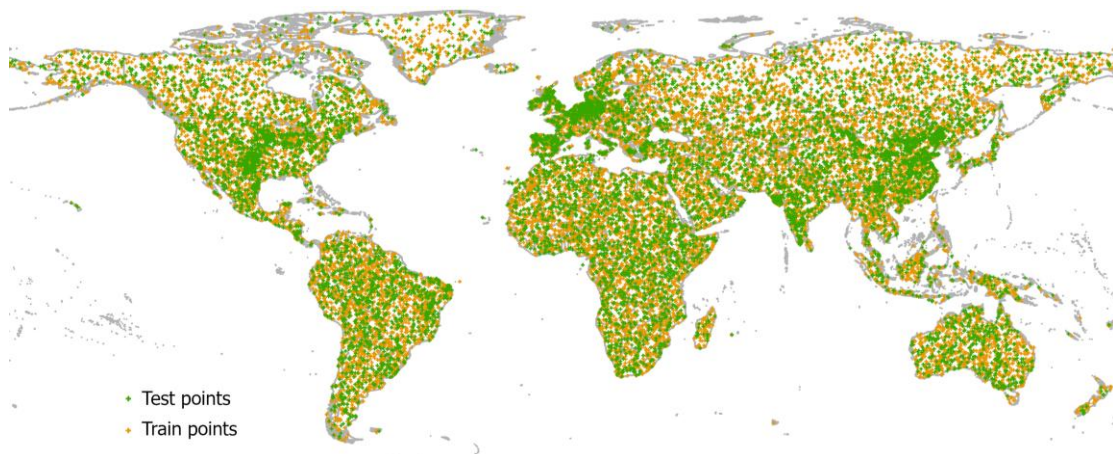
181 Based on the deep learning-classified OSM wind turbine dataset and satellite images,  
 182 we developed an optimized Random Forest model for omission detection (Rigatti,

183 2017). The Random Forest model was trained on GEE using verified wind turbine  
184 locations from OSM, alongside globally sampled negative samples (**Figure 4**). We  
185 employ a global-scale uniform random sampling strategy. This ensured sufficient  
186 spatial separation and geographic diversity among samples, minimizing spatial  
187 dependency and maintaining sample independence. Besides, we apply a 30-meter  
188 buffer around all existing wind turbine locations (positive samples). These buffered  
189 areas are then masked out from the global sampling pool to ensure that no negative  
190 samples are drawn within this exclusion zone. Accordingly, we trained the Random  
191 Forest model with 10,000 globally distributed wind turbine locations (positive samples)  
192 and 20,000 non-turbine points (negative samples). The negative samples are obtained  
193 via globally uniform random sampling to ensure spatial objectivity. The resulting  
194 dataset encompasses diverse land-cover categories, including grasslands, bare land,  
195 cropland, and forests. The dataset was then split into 70% training and 30% testing sets  
196 as illustrated in **Figure 5**.



197

198 **Figure 4.** Spatial distribution of wind turbine (positive) and non-turbine (negative)  
199 training samples for machine learning.



200

201 **Figure 5.** Spatial distribution of train and test datasets for the Random Forest model.  
202 The green ones represent the points selected for model training, and the orange ones  
203 represent the points selected for model testing.

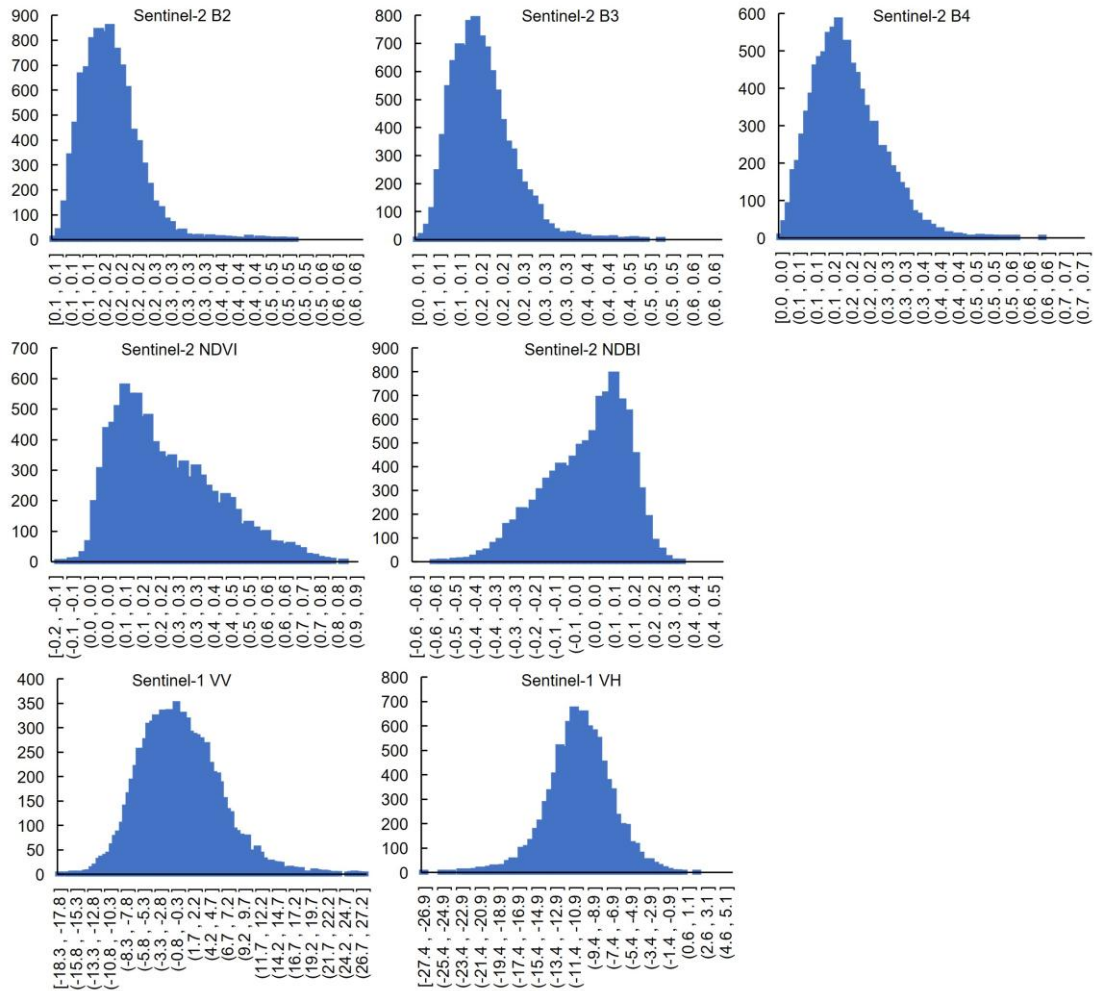
204

205 We constructed a comprehensive feature set for machine learning based on Sentinel-1  
206 and Sentinel-2 satellite imagery integrated via the GEE platform. We utilized the  
207 Sentinel-1 Ground Range Detected (GRD) dataset (COPERNICUS/S1\_GRD),  
208 extracting the VV and VH polarization bands. We employed the Sentinel-2 Surface  
209 Reflectance collection (COPERNICUS/S2\_SR\_HARMONIZED), which includes the  
210 visible and near-infrared (NIR) bands. To ensure data quality, we applied the QA60  
211 band for cloud masking in Sentinel-2 images. Both datasets were processed using a  
212 median reducer across the entire year of 2024 to generate cloud-free, representative  
213 composites. All spectral bands and backscatter coefficients were then normalized to a  
214 range of [0, 1] to mitigate effects from illumination conditions and sensor  
215 characteristics. Finally, these processed layers were stacked into a unified feature  
216 collection to serve as input for the machine learning models.

217 In addition to the original bands from Sentinel-1 and Sentinel-2, we incorporated the  
218 Normalized Difference Vegetation Index (NDVI) (Huang et al., 2021) and the  
219 Normalized Difference Built-up Index (NDBI) (Zha et al., 2003) to enhance the  
220 differentiation between wind turbines and their background features based on the  
221 original bands from Sentinel-2. For comprehensive feature characterization, we  
222 implemented a random sampling strategy across 10,000 wind turbine locations, while  
223 covering all major wind development regions for reliable spectral analysis. **Figure 6**  
224 presents seven selected spectral feature value distributions of wind turbines, revealing  
225 distinct characteristic ranges for turbine signatures across different sensor bands. This  
226 demonstrates the effectiveness of different band features in wind turbine classification.  
227 To reduce the computational load of the Random Forest model, we excluded the 800-  
228 m buffer area of already validated wind turbines and then defined upper and lower  
229 threshold boundaries to filter out non-turbine areas during the initial processing stage.  
230 These thresholds include Sentinel-2's B2 [0, 0.3], B3 [0, 0.3], B4 [0, 0.3], NDVI [0,  
231 0.7], NDBI [0, 0.7], and Sentinel-1's VV [-18, 18] and VH [-25, 1].

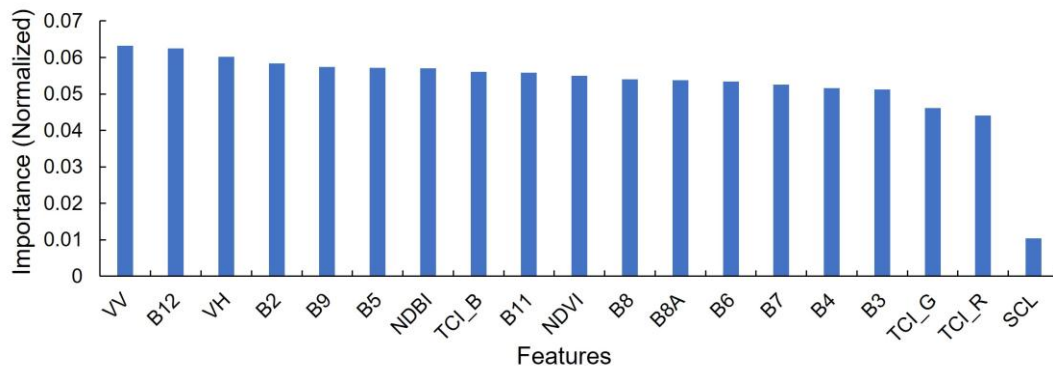
232 The final dataset incorporated 19-dimensional feature data for each sample point, which  
233 was utilized for training the model to detect omitted wind turbine points. Our feature  
234 importance ranking of the 19-dimensional feature space (**Figure 7**) revealed that  
235 Sentinel-1's VV and VH polarization bands are particularly effective for identifying the  
236 wind turbines. This could contribute to the band's high sensitivity to vertical metallic  
237 structures such as wind turbine towers, as these act as corner reflectors that generate  
238 distinct bright signatures in SAR imagery. The Sentinel-2's B12 and B2 bands also show  
239 a strong response to wind turbine structures, which enhances their contrast against  
240 natural backgrounds like vegetation, soil, and water.

241



242

243 **Figure 6.** Feature value distribution of randomly selected wind turbine samples.



244

245 **Figure 7.** Feature importance ranking for building a Random Forest classification  
246 model.

247 **2.3 Classification accuracy assessment of models**

248 We evaluated the performance of both deep learning and traditional machine learning  
249 models using standard classification metrics computed from confusion matrices,  
250 namely precision, recall, and F1-score, as shown in **Eq. (1)-(3)**, as based on an

251 independent test and validation set (Congalton, 1991; Goutte and Gaussier, 2005) to  
252 ensure the model's generalizability and avoid over-optimization on training data.  
253 Producer's accuracy (recall) quantifies the proportion of actual wind turbine locations  
254 correctly detected, while user's accuracy (precision) represents the fraction of predicted  
255 wind turbines that are true positives. The precision equals the number of true positives  
256 (TP) divided by the sum of true positives (TP) and false positives (FP). Where the recall  
257 equals the number of true positives (TP) divided by the sum of true positives (TP) and  
258 false negatives (FN). The F1-score harmonizes these metrics, providing particularly  
259 valuable evaluation for imbalanced wind turbine detection scenarios where background  
260 features significantly outnumber target objects.

$$261 \quad \textit{Precision} = \frac{TP}{TP + FP} \quad (1)$$

$$262 \quad \textit{Recall} = \frac{TP}{TP + FN} \quad (2)$$

$$263 \quad \textit{F1 - score} = 2 \times \frac{\textit{Precision} \times \textit{Recall}}{\textit{Precision} + \textit{Recall}} \quad (3)$$

264 Based on our updated wind turbine dataset, we evaluated the data accuracy and errors  
265 within the OSM wind turbine records. We calculated omission and commission errors  
266 using a spatial proximity analysis in ArcGIS Pro with a 30-meter tolerance buffer. We  
267 applied a 30-m buffer to our generated points and performed a spatial selection on the  
268 OSM reference points to calculate the omission error. And the OSM points not captured  
269 within these buffers were classified as omissions. Conversely, to calculate the  
270 commission error, we buffered the OSM points and identified our generated points that  
271 fell outside these zones. The respective error rates were derived by dividing the count  
272 of omitted or committed points by the total number of OSM wind turbines. Finally,  
273 these two rates were summed to provide a total error rate.

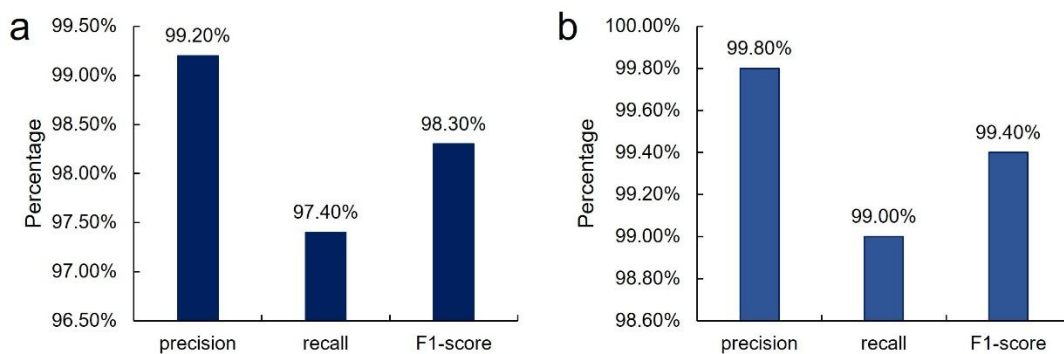
#### 274 **2.4 Land use occupation analysis of onshore wind turbines**

275 We utilize ESRI's 2023 Land Use/Land Cover (LULC) dataset (Karra et al., 2021),  
276 derived from ESA Sentinel-2 images at 10-meter resolution for analyzing the land use  
277 surrounding onshore wind turbines. The LULC composite maps integrate annual  
278 predictions for nine defined categories, namely cropland, rangeland, forest, built-up  
279 areas, bare ground, water bodies, flooded vegetation, snow/ice cover, and cloud cover.  
280 By conducting spatial overlay analysis between our finalized global onshore wind  
281 turbine dataset and the LULC classification within GEE, we characterized land  
282 occupation patterns through the extraction of underlying land use types at wind turbine  
283 sites. Additionally, we evaluated wind turbine land use impacts by conducting an 800-  
284 meter buffer around wind turbines (Dunnett et al., 2020), and converting the results to  
285 raster format for spatial assessment.

### 286 **3 Results**

#### 287 **3.1 Evaluation results**

288 **Figure 8a** displays the deep learning model's performance for onshore wind turbine  
 289 error filtering, achieving exceptional precision (99.2%), recall (97.4%), and F1-score  
 290 (98.3%), respectively. The Random Forest model demonstrated equally strong  
 291 performance, achieving 99.8% recall, 99.0% precision, and 99.4% F1-score (**Figure**  
 292 **8b**). Importantly, the deep learning classifier achieved an 86% reduction in required  
 293 manual verification (291,501 of 339,869 images). Meanwhile, our analysis revealed a  
 294 18.5% error rate in OSM's global wind turbine dataset. The calculated discrepancy is  
 295 yielded from the omission and commission error rates of 14.4% and 4.1%, respectively.  
 296 It is worth noting that this error rate represents global averages, significant regional  
 297 variations could exist as the OSM data fluctuates across different countries due to  
 298 varying mapping efforts. While this validates its reliability for macro-scale trend  
 299 analysis, the findings underscore inherent limitations of data directly obtained from  
 300 OSM for precision-critical wind energy applications.



301

302 **Figure 8.** Evaluation results of two models for wind turbine classification. **(a)** Precision, recall,  
 303 and F1-score of the deep learning model. **(b)** Precision, recall, and F1-score of the traditional  
 304 machine learning model.

305

### 306 3.2 Comparison with open-source datasets

307 To validate the accuracy of our wind turbine records, we cross-validated them against  
 308 multiple authoritative geospatial datasets, including the 2020 global wind and solar  
 309 dataset (Dunnett et al., 2020), along with official and research-based wind turbine  
 310 inventories from the United States (Rand et al., 2020), Italy (Smeraldo et al., 2020),  
 311 Germany (Manske et al., 2022), and South Africa (Kleebauer et al., 2025). Our dataset  
 312 (GonshoreWT2024) documents 416,532 wind turbines (**Table 1**), representing a tenfold  
 313 expansion from the 2020 baseline of 33,514 wind turbines. The wind turbine counts of  
 314 GonshoreWT2024 closely align with Global Renewables Watch (375,197 wind  
 315 turbines), with a 9.9% variance. The consistency between our estimates and official  
 316 records for temporally comparable years is high, with discrepancies of less than 2.3%  
 317 in the United States and less than 0.3% in South Africa. This also provides strong  
 318 validation of our methodology's precision. Our cross-validation across multiple data  
 319 sources and regions reveals both remarkable consistency and a substantial quantity of  
 320 previously unrecorded wind turbine installations.

321 **Table 1.** Comparison of open-source datasets of wind turbines with our results.

Scope	Time	Number	Ours (2024)
Dunnett et al. (2020)	2020	33,514	416,532
Global Renewables Watch (Robinson et al., 2025)	2024(Quarter 2)	375,197	416,532
United States (Rand et al., 2020)	2024	75,781	74,052
Germany (Manske et al., 2022)	2021	28,156	29,971
Italy (Smeraldo et al., 2020)	2020	8,729	10,591
South Africa (Kleebauer et al., 2025)	2025	1,487	1,483

322

323 We further benchmark our dataset against the current global-scale wind turbine datasets,  
 324 including Dunnett et al. (2020) and Global Renewables Watch (**Table 2**). Results show  
 325 that our dataset contains the largest number of identified onshore wind turbines while  
 326 maintaining nation-level coverage and land type classification compared to Dunnett et  
 327 al. (2020). In terms of data records, the Global Renewables Watch is updated to the  
 328 second quarter of 2024 with 375,197 wind turbines and includes a limited number of  
 329 offshore wind turbines that are not comprehensively. Our dataset focuses on onshore  
 330 wind turbines and incorporates additional updates by the end of 2024. Methodologically,  
 331 the Global Renewables Watch requires massive training datasets and substantial  
 332 computational resource budget exceeding 650 V100 GPU hours to process around 14  
 333 terapixels of satellite imagery (Robinson et al., 2025). In contrast, our hybrid  
 334 framework utilizes medium-to-high resolution imagery to enable global-scale updates  
 335 with significantly lower computational demands. By leveraging publicly available  
 336 platforms, this framework lowers the barrier to entry through a cost-effective and  
 337 resource-efficient alternative.

338 **Table 2.** Comparisons with current global-scale wind turbine datasets.

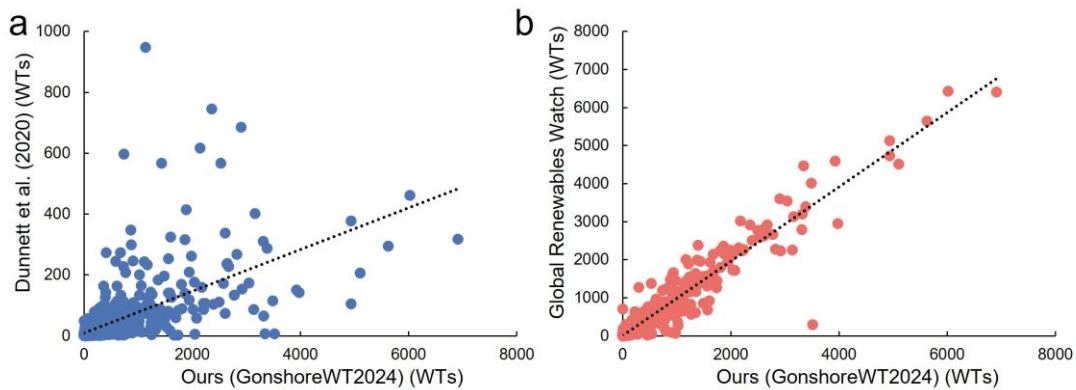
Scope	Technology	Time	Number	Onshore number	Land type	Nation	Construction year	Updating algorithm
Dunnett et al. (2020)	Onshore and part Offshore	2020	33,514	33,240	No	Yes	No	No
Global Renewables Watch (Robinson et al., 2025)	Onshore and part Offshore	2024 (Quarter 2)	375,197	373,577	Yes	Yes	Yes	Yes
Ours (GonshoreWT2024)	Onshore	2024	416,532	416,532	Yes	Yes	No	Yes

339

340 We also conducted a spatial distribution analysis to assess the correlation between our  
 341 dataset and existing benchmarks, including the Dunnett et al. (2020) and Global  
 342 Renewables Watch. Specifically, the global study area was partitioned into  $2^\circ \times 2^\circ$  grid  
 343 cells to calculate wind turbine counts. We then employed scatter plots to evaluate the

344 spatial consistency of our dataset relative to Dunnett et al. (2020) and the Global  
 345 Renewables Watch (**Figure 9**). Subsequently, Pearson's  $r^2$  is calculated to quantify the  
 346 correlation between the datasets. Our dataset shows a moderate correlation with  
 347 Dunnett et al. (2020) (**Figure 9a**), with a Pearson's  $r^2$  of 0.4, primarily due to the  
 348 significantly expanded coverage of our dataset. In contrast, our dataset shows a high  
 349 correlation with Global Renewables Watch with a Pearson  $r^2$  of 0.93, indicating a high  
 350 degree of geospatial consistency (**Figure 9b**).

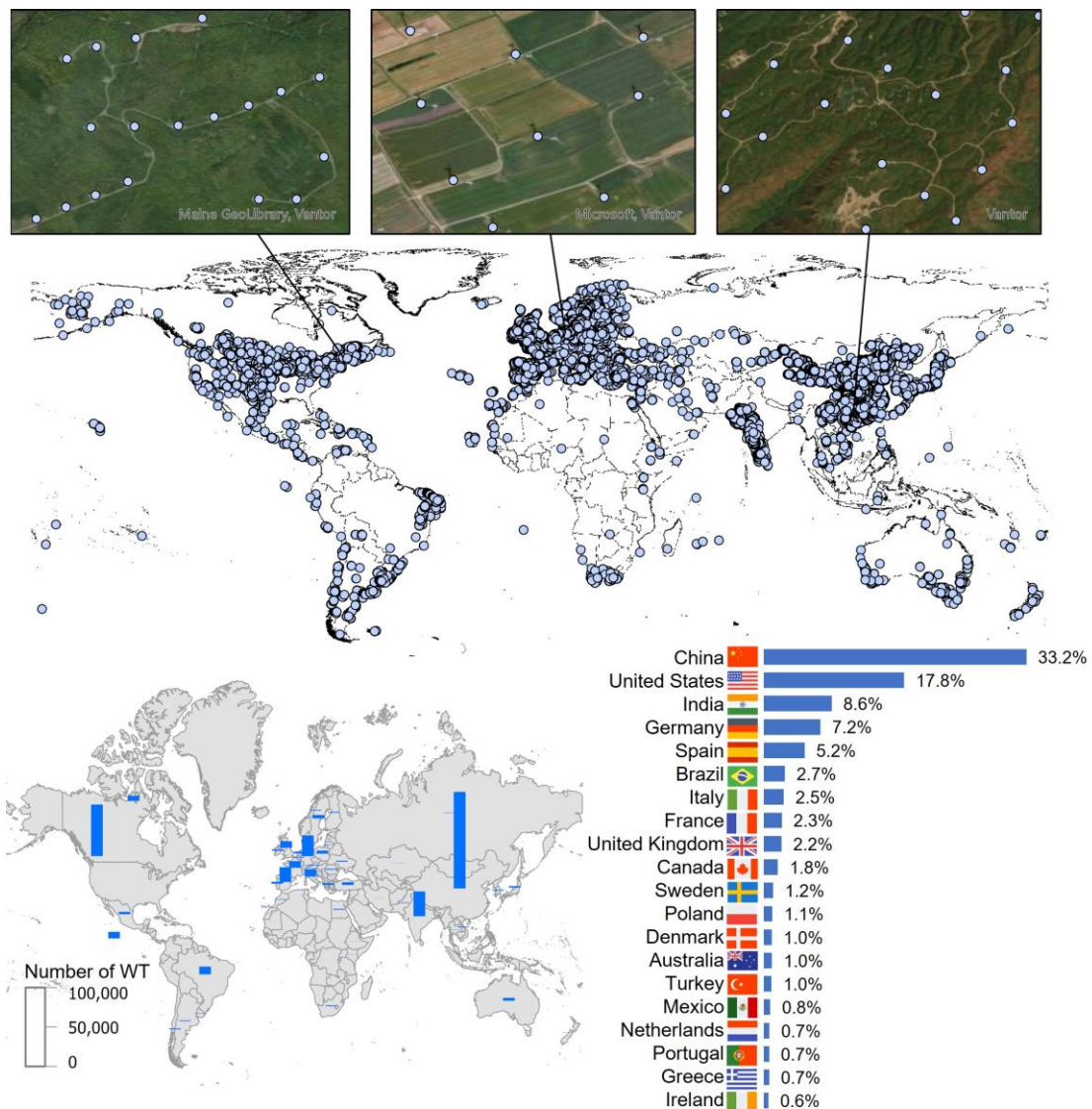
351 Additionally, we quantified the mutual global underreporting between Global  
 352 Renewables Watch and ours, which is around 20%. Global Renewables Watch has  
 353 72,304 more different wind turbines than ours, and we have 80,532 more different wind  
 354 turbines than theirs. We further conduct manual verification to quantify omission and  
 355 commission rates of our dataset in these wind turbines. Final verification shows a 59%  
 356 validity rate (43,011/72,304) for unique wind turbine entries of Global Renewables  
 357 Watch, compared to a 92% validity rate (74,458/80,532) for ours. We further updated  
 358 our dataset to a final global count of 416,532 wind turbines based on manual  
 359 verification.



360  
 361 **Figure 9.** Global grid-based ( $2^\circ \times 2^\circ$ ) correlation analysis of our dataset (GonshoreWT2024)  
 362 and existing benchmarks. **(a)** Distribution of grid-level wind turbine counts between our dataset  
 363 (GonshoreWT2024) and Dunnett et al. (2020). **(b)** Distribution of grid-level wind turbines  
 364 between our dataset (GonshoreWT2024) and Global Renewables Watch.

### 365 3.3 Global onshore wind turbine installation distribution

366 The finalized global dataset (GonshoreWT2024) contains 416,532 georeferenced wind  
 367 turbines exhibiting pronounced concentration across northern hemisphere regions  
 368 (**Figure 10a**), particularly in North America, Europe, and East Asia. Regional  
 369 deployment patterns also show clear geographic concentrations (**Figure 10b**). China  
 370 dominates global wind energy deployment, with 138,486 wind turbines representing  
 371 33.2% of worldwide installations. The United States ranks second (74,051 wind  
 372 turbines), followed by India (35,783), Germany (29,970), and Spain (21,543),  
 373 collectively representing the top five national markets (**Figure 10c**). China and India,  
 374 representing 75% of Asia's wind turbine installations, and the United States and Brazil  
 375 together comprise 77% of American deployments. Europe's wind energy deployment  
 376 is primarily concentrated in Germany, Spain, and Italy, which account for 40% of



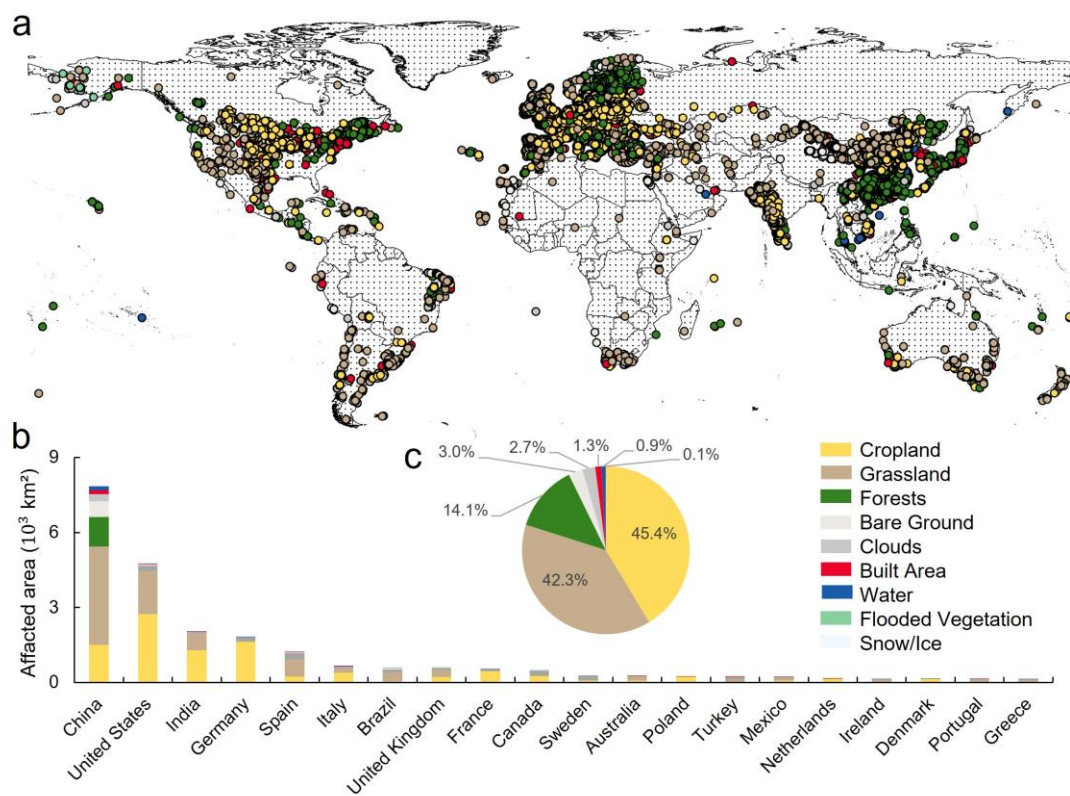
378

379 **Figure 10.** Global onshore wind turbine installation records and spatial distribution. (a)  
 380 Global onshore wind turbine by 2024. (b) Spatial distribution of wind turbine  
 381 installation statistics by country. (c) Percentage ranking of wind turbines for top 20  
 382 countries.

### 383 3.4 Land use types and spatial distribution of global onshore wind turbines

384 Our global assessment quantifies a total impacted area of 367,132 km<sup>2</sup> of the wind  
 385 turbines, which is estimated with an 800-meter buffer around wind turbine locations  
 386 (Dunnett et al., 2020). Among the affected areas, 87% of wind turbines are located  
 387 within cropland and grassland ecosystems (**Figure 11c**). Specifically, croplands  
 388 represent the predominant land use at 45% (165,209 km<sup>2</sup>), followed by grasslands for  
 389 42% (154,195 km<sup>2</sup>), and forests for 14% (51,398 km<sup>2</sup>). These proportions, however,  
 390 exhibit substantial variation across national boundaries (**Figure 11a, b**). China, the  
 391 global leader in wind capacity, exhibits unique siting patterns with over 50% of wind

392 turbines deployed in grasslands, followed by croplands (20%) and forests (16%). China  
 393 demonstrates a notably higher reliance on forested areas for wind turbine siting  
 394 compared to global patterns, particularly in its southern provinces (**Figure 11a**),  
 395 warranting careful ecological assessment (Enevoldsen, 2016). In contrast, the United  
 396 States distributes roughly half (50%) of its wind turbines across croplands,  
 397 supplemented by grassland deployments. Germany displays the most extreme  
 398 geographic specialization, with over 90% of its wind turbines sited exclusively on  
 399 agricultural lands. These pronounced regional variations in wind turbine siting patterns  
 400 carry significant implications for both renewable energy development and landscape  
 401 management policies.



402

403 **Figure 11.** Land use distribution of global onshore wind turbines. **(a)** Land use distribution of  
 404 global onshore wind turbines. **(b)** Land use area statistics occupied by onshore wind turbines  
 405 by country. **(c)** Percentages of difference in land use deployed by onshore wind turbines.

406 **3.5 Potential applications of the dataset**

407 This open-access global onshore wind turbine dataset (GonshoreWT2024) could  
 408 establish a critical foundation for interdisciplinary research, facilitating integrated  
 409 studies in energy infrastructure planning, ecological impact evaluation, and land use  
 410 optimization. First, the geospatial wind turbine dataset enables rigorous biodiversity  
 411 impact assessments, including wildlife disturbance patterns and habitat fragmentation  
 412 analysis around wind energy installations (Bopucki and Perzanowski, 2018; McKay et  
 413 al., 2024). Particularly, studies have demonstrated that turbine blade rotation creates  
 414 distinct mortality patterns across bird and bat species (Marques et al., 2020; Millon et

415 al., 2018). Our precisely geolocated turbine records enable exact spatial correlation  
416 between wind infrastructure and vulnerable species' high-activity areas, facilitating  
417 data-driven assessments of avian and chiropteran collision risks.

418 Second, wind farm construction and associated infrastructure development induce  
419 significant ecological disruptions through multiple pathways (Xia et al., 2025).  
420 Integrating high-precision turbine locations with remote sensing data allows systematic  
421 evaluation of wind energy's environmental footprint, including deforestation patterns  
422 (Enevoldsen, 2018), soil erosion (Ma et al., 2023), and carbon sink loss (Gao et al.,  
423 2023). Our dataset provides a robust data foundation for both evaluating the cumulative  
424 ecological impacts of existing wind farms and optimizing future turbine siting to  
425 balance energy production with ecosystem conservation.

## 426 **4 Data availability**

427 These open-access data resources could help promote transparent and just sustainable  
428 wind energy development, and enable detailed feature extraction and spatial analysis  
429 for future wind energy research. The global onshore wind turbine dataset  
430 (GonshoreWT2024) is freely available from the Zenodo website at:  
431 <https://doi.org/10.5281/zenodo.18984175> (Shujun et al., 2025).

432 The dataset includes:

- 433 ● A comprehensive global inventory of 416,532 onshore wind turbines in the format  
434 of a geospatial shapefile. The dataset includes geolocation coordinates for all wind  
435 turbines, along with corresponding nation (Field: 'Nation') and land use  
436 classification (Field: 'landtype') for each wind turbine.

437 The code file includes:

- 438 ● A PyTorch-based ResNet-18 implementation for classifying onshore wind turbines  
439 in Google Earth images, including codes for model architecture and pre-trained  
440 weights.
- 441 ● The GEE-based code for the Random Forest model, including sample point  
442 splitting (training/test sets) and model training.

## 443 **5 Discussion and conclusion**

444 This study introduces an advanced geospatial approach that integrates high-resolution  
445 Google Earth images with multi-source satellite observations to construct a refined  
446 global inventory of onshore wind turbines. Compared to the current datasets of  
447 available global onshore wind turbines, our dataset provides more timely data that  
448 represents a tenfold expansion over the global wind turbine inventories as of 2020.  
449 Importantly, in mapping methodology, compared to the new updating framework of  
450 Global Renewables Watch, we propose a reproducible and straightforward approach to  
451 identify renewable infrastructure, which can be applied in future studies and in  
452 countries or regions with limited computational resources. The datasets and resulting

453 2024 global inventory document 416,532 onshore wind turbines, serving as a critical  
454 resource for renewable energy infrastructure planning and ecological impact studies.

455 The global analysis demonstrates significant spatial aggregation of wind turbines, with  
456 the densest concentrations occurring in northern mid-latitude zones, particularly high-  
457 density concentrations in Europe, North America, and East Asia. This spatial  
458 concentration pattern stems from factors including optimal wind resources (Davis et al.,  
459 2023; Liu et al., 2023), supportive policy frameworks (Godby et al., 2025; Kumar et al.,  
460 2022; Liao, 2016), and established energy infrastructure networks (Oró et al., 2015;  
461 Rochmińska, 2023) prevalent in these mid-latitude zones. Notably, the global wind  
462 energy has developed across 367,132 km<sup>2</sup> of land, with croplands (45%) and grasslands  
463 (42%) hosting the majority (87%) of turbine installations. This distribution reflects a  
464 strategic preference for siting turbines in previously developed or ecologically low-  
465 sensitivity areas. However, the associated ecological impacts, particularly habitat  
466 fragmentation and soil disturbance, require thorough environmental evaluation and  
467 mitigation planning (Moore O'Leary et al., 2017).

468 Wind turbines primarily appear as point features in satellite images, presenting  
469 significant challenges for automated large-scale detection (Zhai et al., 2024). These  
470 detection challenges are further intensified by visually similar infrastructure,  
471 particularly high-voltage transmission lines and isolated structures that mimic turbine  
472 signatures. Our proposed solution combines hybrid machine/deep learning  
473 architectures with systematic sampling approaches to enable reliable turbine  
474 identification across diverse terrain types. Looking ahead, sustainable renewable energy  
475 development, including wind, solar, and hydropower, requires continuous innovation  
476 and open geospatial data to enhance planning transparency and governance. Overall,  
477 our framework offers a novel approach and solution for cost-effective, timely updates  
478 of global onshore wind turbine data.

479 **Author contributions.** SL and PW designed the study and wrote the original  
480 manuscript. SL designed the methods and carried out the experiments and validation.  
481 JQ and YS edited and revised the paper.

482 **Competing interests.** The contact author has declared that none of the authors has any  
483 competing interests.

484 **Disclaimer.** Publisher's note: Copernicus Publications remains neutral with regard to  
485 jurisdictional claims in published maps and institutional affiliations.

486 **Acknowledgements.** The authors are grateful to the ESA's Copernicus program for  
487 providing free access to the Sentinel-1/2 data and the Google Earth Engine platform for  
488 preprocessing and making the data accessible. We also thank OpenStreetMap for  
489 providing global onshore wind turbine locations and the land polygon data.

490 **Financial support.** This work was supported by the National Key Research and  
491 Development Program (Grant No.2023YFC3904500).

492

493 **References**

494 Bopucki, R. and Perzanowski, K.: Effects of wind turbines on spatial distribution of the  
495 European hamster, *Ecol. Indic.*, 84, 433-436, 2018.

496 Calvert, K., Pearce, J. M., and Mabee, W. E.: Toward renewable energy geo-information  
497 infrastructures: applications of giscience and remote sensing that build institutional capacity,  
498 *Renewable and Sustainable Energy Reviews*, 18, 416-429, 2013.

499 Cerri, J., Costantino, C., De Rosa, D., Banič, D. A., Urgeghe, G., Fozzi, I., Echeverria, J., Aresu,  
500 M., and Berlinguer, F.: Widely used datasets of wind energy infrastructures can seriously  
501 underestimate onshore turbines in the Mediterranean, *Biol. Conserv.*, 300, 110870, 2024.

502 Congalton, R. G.: A review of assessing the accuracy of classifications of remotely sensed data,  
503 *Remote Sens. Environ.*, 37, 35-46, 1991.

504 Dai, T., Jose Valanarasu, J. M., Zhao, Y., Zheng, S., Sun, Y., Patel, V. M., and Jordaan, S. M.:  
505 Land resources for wind energy development require regionalized characterizations, *Environ.*  
506 *Sci. Technol.*, 58, 5014-5023, 2024.

507 Davis, N. N., Badger, J., Hahmann, A. N., Hansen, B. O., Mortensen, N. G., Kelly, M., Larsén,  
508 X. G., Olsen, B. T., Floors, R., and Lizcano, G.: The global wind atlas: a high-resolution dataset  
509 of climatologies and associated web-based application, *Bull. Amer. Meteorol. Soc.*, 104,  
510 E1507-E1525, 2023.

511 Dunnett, S., Sorichetta, A., Taylor, G., and Eigenbrod, F.: Harmonised global datasets of wind  
512 and solar farm locations and power, *Sci. Data*, 7, 130, 2020.

513 Effenberger, N. and Ludwig, N.: A collection and categorization of open - source wind and  
514 wind power datasets, *Wind Energy*, 25, 1659-1683, 2022.

515 Enevoldsen, P.: Onshore wind energy in northern European forests: reviewing the risks,  
516 *Renewable and Sustainable Energy Reviews*, 60, 1251-1262, 2016.

517 Enevoldsen, P.: A socio-technical framework for examining the consequences of deforestation:  
518 a case study of wind project development in northern Europe, *Energy Policy*, 115, 138-147,  
519 2018.

520 Gao, L., Wu, Q., Qiu, J., Mei, Y., Yao, Y., Meng, L., and Liu, P.: The impact of wind energy  
521 on plant biomass production in China, *Sci. Rep.*, 13, 22366, 2023.

522 Godby, R., Cook, B., Holland, M., and Kjorstad, T.: State incentives: impact on wind energy  
523 costs and policy development, *Renewable and Sustainable Energy Reviews*, 215, 115572, 2025.

524 Goutte, C. and Gaussier, E.: A probabilistic interpretation of precision, recall and f-score, with  
525 implications for evaluation, in: *European Conference on Information Retrieval*, Springer, 345-  
526 359, 2005.

527 He, K., Zhang, X., Ren, S., and Sun, J.: Deep residual learning for image recognition, in:  
528 *Proceedings of the IEEE conference on computer vision and pattern recognition*, IEEE, Las  
529 Vegas, NV, USA, 770-778, 2016.

530 Hoeser, T., Feuerstein, S., and Kuenzer, C.: Deepowl: a global offshore wind turbine data set  
531 derived with deep learning from Sentinel-1 data, *Earth System Science Data Discussions*, 2022,  
532 1-26, 2022.

533 Huang, S., Tang, L., Hupy, J. P., Wang, Y., and Shao, G.: A commentary review on the use of  
534 normalized difference vegetation index (NDVI) in the era of popular remote sensing, *J. For.*  
535 *Res.*, 32, 1-6, 2021.

536 Karra, K., Kontgis, C., Statman-Weil, Z., Mazzariello, J. C., Mathis, M., and Brumby, S. P.:  
537 Global land use/land cover with Sentinel-2 and deep learning, in: *2021 IEEE International*

538 Geoscience and Remote Sensing Symposium IGARSS, IEEE, Brussels, Belgium, 4704-4707,  
539 2021.

540 Kati, V., Kassara, C., Vrontisi, Z., and Moustakas, A.: The biodiversity-wind energy-land use  
541 nexus in a global biodiversity hotspot, *Sci. Total Environ.*, 768, 144471, 2021.

542 Kleebauer, M., Karamanski, S., Callies, D., and Braun, M.: A wind turbines dataset for South  
543 Africa: OpenStreetMap data, deep learning based geo-coordinate correction and capacity  
544 analysis, *Isprs Int. J. Geo-Inf.*, 14, 232, 2025.

545 Kruitwagen, L., Story, K. T., Friedrich, J., Byers, L., Skillman, S., and Hepburn, C.: A global  
546 inventory of photovoltaic solar energy generating units, *Nature*, 598, 604-610, 2021.

547 Kumar, A., Pal, D., Kar, S. K., Mishra, S. K., and Bansal, R.: An overview of wind energy  
548 development and policy initiatives in India, *Clean Technol. Environ. Policy*, 24, 1337-1358,  
549 2022.

550 Liao, Z.: The evolution of wind energy policies in China (1995 – 2014): an analysis based on  
551 policy instruments, *Renewable and Sustainable Energy Reviews*, 56, 464-472, 2016.

552 Liu, Y., Feng, S., Qian, Y., Huang, H., and Berg, L. K.: How do North American weather  
553 regimes drive wind energy at the sub-seasonal to seasonal timescales? *Npj Clim. Atmos. Sci.*,  
554 6, 100, 2023.

555 Ma, B., Yang, J., Chen, X., Zhang, L., and Zeng, W.: Revealing the ecological impact of low-  
556 speed mountain wind power on vegetation and soil erosion in South China: a case study of a  
557 typical wind farm in Yunnan, *J. Clean. Prod.*, 419, 138020, 2023.

558 Manske, D., Grosch, L., Schmiedt, J., Mittelstädt, N., and Thrän, D.: Geo-locations and system  
559 data of renewable energy installations in Germany, *Data*, 7, 128, 2022.

560 Marques, A. T., Santos, C. D., Hanssen, F., Muñoz, A. R., Onrubia, A., Wikelski, M., Moreira,  
561 F., Palmeirim, J. M., and Silva, J. P.: Wind turbines cause functional habitat loss for migratory  
562 soaring birds, *J. Anim. Ecol.*, 89, 93-103, 2020.

563 Mckay, R. A., Johns, S. E., Bischof, R., Matthews, F., van der Kooij, J., Yoh, N., and Eldegard,  
564 K.: Wind energy development can lead to guild - specific habitat loss in boreal forest bats,  
565 *Wildlife Biol.*, 2024, e1168, 2024.

566 Mckenna, R., Lilliestam, J., Heinrichs, H. U., Weinand, J., Schmidt, J., Staffell, I., Hahmann,  
567 A. N., Burgherr, P., Burdack, A., and Bucha, M.: System impacts of wind energy developments:  
568 key research challenges and opportunities, *Joule*, 9, 2025.

569 Millon, L., Colin, C., Brescia, F., and Kerbiriou, C.: Wind turbines impact bat activity, leading  
570 to high losses of habitat use in a biodiversity hotspot, *Ecol. Eng.*, 112, 51-54, 2018.

571 Mishra, M., Desul, S., Santos, C. A. G., Mishra, S. K., Kamal, A. H. M., Goswami, S., Kalumba,  
572 A. M., Biswal, R., Da Silva, R. M., and Dos Santos, C. A. C.: A bibliometric analysis of  
573 sustainable development goals (sdgs): a review of progress, challenges, and opportunities,  
574 *Environment, Development and Sustainability*, 26, 11101-11143, 2024.

575 Moore O'Leary, K. A., Hernandez, R. R., Johnston, D. S., Abella, S. R., Tanner, K. E., Swanson,  
576 A. C., Kreidler, J., and Lovich, J. E.: Sustainability of utility - scale solar energy - critical  
577 ecological concepts, *Front. Ecol. Environ.*, 15, 385-394, 2017.

578 Muller, E., Gremmo, S., Houtin-Mongrolle, F., Duboc, B., and Bénard, P.: Field-data-based  
579 validation of an aero-servo-elastic solver for high-fidelity large-eddy simulations of industrial  
580 wind turbines, *Wind Energy Sci.*, 9, 25-48, 2024.

581 Oró, E., Depoorter, V., Garcia, A., and Salom, J.: Energy efficiency and renewable energy

582 integration in data centres. Strategies and modelling review, *Renewable and Sustainable Energy*  
583 *Reviews*, 42, 429-445, 2015.

584 Raimi, D., Zhu, Y., Newell, R. G., Prest, B. C., and Bergman, A.: Global energy outlook 2023:  
585 sowing the seeds of an energy transition, *Resour. Future*, 1, 1-44, 2023.

586 Rand, J. T., Kramer, L. A., Garrity, C. P., Hoen, B. D., Diffendorfer, J. E., Hunt, H. E., and  
587 Spears, M.: A continuously updated, geospatially rectified database of utility-scale wind  
588 turbines in the United States, *Sci. Data*, 7, 15, 2020.

589 Rigatti, S. J.: Random Forest, *Journal of Insurance Medicine*, 47, 31-39, 2017.

590 Rinne, E., Holttinen, H., Kiviluoma, J., and Rissanen, S.: Effects of turbine technology and land  
591 use on wind power resource potential, *Nat. Energy*, 3, 494-500, 2018.

592 Robinson, C., Ortiz, A., Kim, A., Dodhia, R., Zolli, A., Nagaraju, S. K., Oakleaf, J., Kiesecker,  
593 J., and Ferres, J. M. L.: Global renewables watch: a temporal dataset of solar and wind energy  
594 derived from satellite imagery, *Arxiv Preprint Arxiv:2503.14860*, 2025.

595 Rochmińska, A.: Wind energy infrastructure and socio-spatial conflicts, *Energies*, 16, 1032,  
596 2023.

597 Roddis, P., Carver, S., Dallimer, M., Norman, P., and Ziv, G.: The role of community  
598 acceptance in planning outcomes for onshore wind and solar farms: an energy justice analysis,  
599 *Appl. Energy*, 226, 353-364, 2018.

600 Shujun, L., Jianchuan, Q., Yongze, S., and Wang, P.: Mapping global onshore wind turbines  
601 using multi-source remote sensing images and hybrid learning approaches, 2025.

602 Smeraldo, S., Bosso, L., Fraissinet, M., Bordignon, L., Brunelli, M., Ancillotto, L., and Russo,  
603 D.: Modelling risks posed by wind turbines and power lines to soaring birds: the black stork  
604 (*Ciconia Nigra*) in Italy as a case study, *Biodivers. Conserv.*, 29, 1959-1976, 2020.

605 Tavakkoli, S., Macknick, J., Heath, G. A., and Jordaan, S. M.: Spatiotemporal energy  
606 infrastructure datasets for the United States: a review, *Renewable and Sustainable Energy*  
607 *Reviews*, 152, 111616, 2021.

608 Xia, Z., Li, Y., Guo, S., Zhang, X., Pan, X., Fang, H., Chen, R., and Du, P.: Assessment of  
609 forest disturbance and soil erosion in wind farm project using satellite observations, *Resources,*  
610 *Conservation and Recycling*, 212, 107934, 2025.

611 Zha, Y., Gao, J., and Ni, S.: Use of normalized difference built-up index in automatically  
612 mapping urban areas from tm imagery, *Int. J. Remote Sens.*, 24, 583-594, 2003.

613 Zhai, Y., Chen, X., Cao, X., and Cui, X.: Identifying wind turbines from multiresolution and  
614 multibackground remote sensing imagery, *Int. J. Appl. Earth Obs. Geoinf.*, 126, 103613, 2024.

615 Zhang, T., Tian, B., Sengupta, D., Zhang, L., and Si, Y.: Global offshore wind turbine dataset,  
616 *Sci. Data*, 8, 191, 2021.

617